FULL PAPER

# An Analytic Model for the Dielectric Function of Au, Ag, and their Alloys

*David Rioux, Simon Vallières, Sébastien Besner, Philip Muñoz, Eric Mazur, and Michel Meunier**

**An analytical model for the prediction of the dielectric properties of gold–silver alloys is developed. This multi-parametric model is a modification of the usual Drude–Lorentz model that takes into account the band structure of the metals. It is fitted by a genetic algorithm to the dielectric function of thin alloy films of different gold–silver ratio obtained by ellipsometry. The model is validated for arbitrary alloy compositions by comparing the experimental extinction spectra of alloy nanoparticles with the spectra predicted by Mie theory.**

## 1. Introduction

Gold and silver plasmonic nanoparticles (NPs) are widely used in biological applications, such as contrast agents for cancer detection,[1–3] photothermal therapy,[1,4,5,5] or energy-intermediate materials in nanosurgery.[6] Their use relies on the strong interaction of light with surface plasmons, which give rise to very high extinction coefficients and significant amplification of the electric field near the metallic surface. This near-field enhancement is also the underlying mechanism for many applications, including surface-enhanced Raman scattering (SERS) and surface-enhanced fluorescence (SEF).[7] The strong sensitivity of surface plamons to the refractive index in the vicinity of the metallic surface also led to the development of surface plasmon resonance (SPR) sensing.[8]

Although gold and silver are both excellent plasmonic materials, they each have a fixed plasmon resonance for a given geometry, which limits the possible applications of either material. Gold–silver alloys, on the other hand, hold great promise because their plasmonic resonance wavelength can be tuned by changing the alloy composition. It is therefore possible to engineer the alloy composition that will meet the required resonance wavelength for any application.

D. Rioux, S. Vallières, Dr. S. Besner, Prof. M. Meunier
Laser Processing and Plasmonics Laboratory
Engineering Physics Department
École Polytechnique de Montréal
C.P. 6079, Succ. Centre-ville, Montréal
Québec, H3C 3A7, Canada
E-mail: michel.meunier@polymtl.ca
P. Muñoz, Prof. E. Mazur
School of Engineering and Applied Sciences
Harvard University
9 Oxford Street, Cambridge, Massachusetts, 02138, USA

**DOI: 10.1002/adom.201300457**

For all applications, it is highly desirable to predict the optical properties of the material prior to synthesis. Calculation of these optical properties is possible with analytical or numerical solutions depending on the complexity of the nanostructure geometry. In all cases, the frequency-dependent dielectric function ($\varepsilon(\omega)$) of the materials making up the nanostructure must be known. Whereas the dielectric functions for pure elements like gold and silver ($\varepsilon_{Au}$ and $\varepsilon_{Ag}$) have been measured extensively and known for years,[9–11] the dielectric function for their alloys ($\varepsilon_{AuAg}$) is relatively unknown. Some specific alloy compositions have been measured, but only over a limited wavelength range.[12] Other more complete measurements have been made,[13] but access to tabulated data is limited. While a clear understanding of the variation of $\varepsilon_{AuAg}$ with alloy composition has not yet been achieved, such knowledge is essential for the predictive engineering of the surface plasmon resonance.

A simple composition-weighted average of $\varepsilon_{Au}$ and $\varepsilon_{Ag}$ does not yield acceptable results, and is not physically realistic for alloys. For example, the extinction spectra of real alloy nanoparticles show a single and relatively narrow plasmon peak with a position varying linearly with alloy composition; both properties are not predicted by the composition-weighted average model.[14,15] Gaudry et al.[14] observed a smooth transition from $\varepsilon_{Au}$ to $\varepsilon_{Ag}$ as a function of alloy composition. They suggested a more complex approach using a linear variation for the interband transition threshold. This approach gives better results for the interband part of the dielectric function, but does not account for the change in the free electron behaviour of alloys of varying composition.

Moskovits et al.[16] attempted to extract $\varepsilon_{AuAg}$ from the extinction spectrum of bimetallic Au–Ag nanoparticles with various compositions, however, it is not clear if their nanoparticles were really alloys or simply core–shells.

In this paper, we present a better model that describes $\varepsilon_{AuAg}$ over the whole visible range and accounts for the smooth transition observed in $\varepsilon$. We fit this model to the measured $\varepsilon(\omega)$ of five thin films with different Au–Ag alloy compositions to obtain an empirical multi-parametric equation of the dielectric function. We compute the extinction spectra of alloy nanoparticles predicted by incorporating this model of $\varepsilon(\omega)$ into Mie theory. The comparison between these spectra and experimental spectra of alloy nanoparticles shows excellent agreement on the position and width of the extinction peaks.

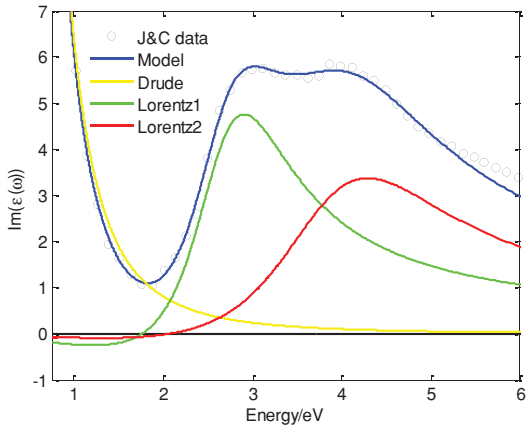


**Figure 1.** Fit of the Au dielectric function based on modified Lorentzian functions. The negative absorption is clearly seen below 2 eV for the first modified Lorentzian term (green curve) and is also present below 1.5 eV for the second one (red curve).[18,19]

## 2. Theoretical Model

For metals, $\varepsilon$ is usually modelled using a Drude–Lorentz approach. The Drude term accounts for the intraband behaviour and is characterized by two parameters: the plasma frequency and a broadening factor related to the free electron lifetime. The interband contribution is usually modelled using one or more Lorentzian oscillators.[16,17] A good quality fit of $\varepsilon$ often requires the use of an exceedingly large number of arbitrary Lorentzian terms and the model becomes unphysical.[18] A different model for the interband contribution is therefore required.

Based on a critical point analysis of the metal band structure, Etchegoin et al.[18,19] have proposed a model of the interband contribution using two modified Lorentzian functions which include a phase parameter in order to account for the band-edge effects.[20] They fitted the model to experimental $\varepsilon_{Au}$ values measured by Johnson and Christy.[9] This fit is shown in **Figure 1** (only the imaginary part of $\varepsilon_{Au}$ is shown). Although this approach closely approximates the data, it may introduce unphysical effects: the phase parameter can cause the imaginary part of $\varepsilon$ for one or both of these modified Lorentzian functions to become negative, which is impossible for a metal. This is the case in Figure 1, where the second Lorentzian term (green) is negative at energies below 2 eV. In order to compensate for this, the Drude term (yellow) must be artificially higher than normal. For these reasons, we consider this model to be unphysical and will not use it.

Despite the difficulties of the previous model, the idea of building a model based on critical point analysis is promising, provided that negative absorption is prevented. Critical point analysis is based on the fact that the most important features in $\varepsilon$ are due to the Van Hove singularities (critical points) in the joint density of states (jDOS). If we can model the jDOS in the energy range of visible light, we can model $\varepsilon$.

According to Cardona,[21] the interband contribution ($\varepsilon_{ib}$) to the complex dielectric function is given by:

$$\in_{ib}(\omega) = 4\pi \sum_{\substack{l\ empty \\ k\ occuppied}} \frac{F_{lk}}{\omega_{lk}^2 - (\omega + i\Gamma)^2} \tag{1}$$

where $k$ and $l$ are the occupied and empty states, respectively. In this model, every transition between an occupied state and an empty state contributes a Lorentzian oscillator to the dielectric function, where $\hbar\omega_{lk}$ is the energy of the transition between both states, $F_{lk}$ is the oscillator strength, and $\Gamma$ is a broadening factor due to scattering. Summation of all the transitions results in the total interband contribution to the dielectric function.

In this model, the oscillator strength is:

$$F_{lk}(\omega) = \frac{2|\langle k|\, p\,|l\rangle|^2}{3\omega_{lk}} \tag{2}$$

We assume that the matrix element in the oscillator strength varies slowly around the critical points and that the only wavelength dependence comes from the $\omega_{lk}^{-1}$ term.[21] We also assume that $\Gamma$ is constant for each critical point.

Furthermore, by assuming only direct transitions, the summation can be replaced by integration over the jDOS:

$$\in_{ib}(\omega) = A\int_0^\infty \frac{j\,DOS(\omega_{lk})}{\omega_{lk}(\omega_{lk}^2 - (\omega + i\Gamma)^2)} \tag{3}$$

Here, $A$ is an amplitude parameter containing the various constants and the matrix element. Hence, the interband contribution to the dielectric function is a convolution of the jDOS with a simple Lorentzian oscillator whose strength is energy dependent. The main contribution to the shape of the dielectric function is therefore the shape of the jDOS, which itself is mainly affected by the critical points. Consequently, the study of these critical points is important for the calculation of the dielectric function.

Both Au and Ag have a similar electronic structure because of their matching valences, crystal structures, and almost equal lattice constants. In both cases, the relevant critical points in the visible energy range are located at the X and L symmetry points. The band structures of both Au and Ag were calculated by density functional theory around these two symmetry points using the Exciting code[22] and are shown in **Figure 2**. The critical point at X has a gap of about 2.5 eV for Au and 4.0 eV for Ag. In both cases, the critical points are of an $M_1$ type: the critical point is three dimensional with a negative effective mass along one direction (X–Γ in this case). At the L symmetry point, the gap for both metals is about 4.0 eV, and the critical points are of an $M_2$ type: there are negative effective masses along two directions and a positive effective mass along one direction (L–Γ). See Cardona's work[21] for more details.

The gap energy around the critical point can be approximated by a parabolic expansion. In this case, the jDOS for a $M_1$ critical point has the general form:

$$j\,DOS(\omega) \propto \begin{cases} C_1 - \sqrt{\omega_{g1} - \omega} & \text{for } \omega < \omega_{g1} \\ C_1 & \text{for } \omega > \omega_{g1} \end{cases} \tag{4}$$

where $C_1$ is constant.

Of course, at energies lower than the lowest transition energy (arrow labeled $\omega_{01}$ on Figure 2a), the jDOS must be zero. This fixes the value of the constant $C_1$, and the general shape of the jDOS only depends on the values of $\omega_{01}$ and $\omega_{g1}$. In this model, the jDOS continues to infinity, which is a consequence of the fact that the gap energy is described by a parabolic expansion. But since this shape accurately describes the jDOS in the energy

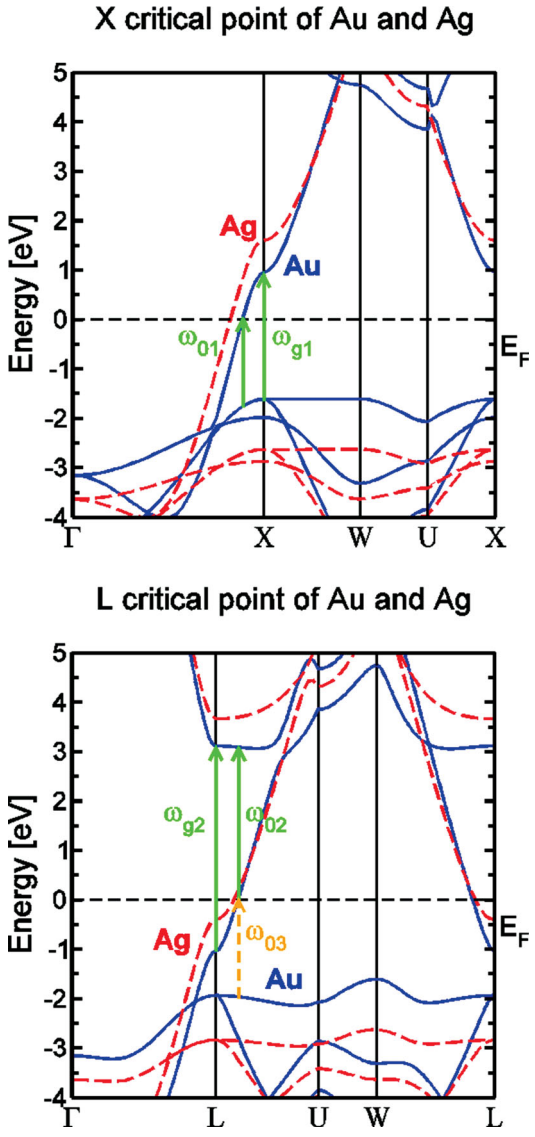


**Figure 2.** Band structure of Au (blue) and Ag (red) near the critical points at the a) X and b) L symmetry points. The green arrows at X represent the threshold ($\omega_{01}$) and gap ($\omega_{g1}$) transitions from the d-bands to the s-band above the Fermi level (FL). The green arrows at L represent the threshold ($\omega_{02}$) and gap ($\omega_{g2}$) transitions from the s-band below the FL to energy levels above the FL. The orange arrow at L represents the threshold ($\omega_{03}$) transition from the d bands to the s band above the FL. As explained in the text, this transition is neglected in our model.

window of interest (1 to 4.5 eV in this work), this approximation is not a problem.

Using Equation (3) and Equation (4), the interband contribution of an $M_1$ critical point to the dielectric function becomes:

$$\epsilon_{CP1}(\omega) = A_1\left[\int_{\omega_{01}}^{\infty}\frac{\sqrt{\omega_{g1}-\omega_{01}}}{\omega_{1k}(\omega_{1k}^2-(\omega+i\Gamma_1)^2)}d\omega_{1k} - \int_{\omega_{01}}^{\omega_{g1}}\frac{\sqrt{\omega_{g1}-\omega_{1k}}}{\omega_{1k}(\omega_{1k}^2-(\omega+i\Gamma_1)^2)}d\omega_{1k}\right] \quad (5)$$

After integration, we obtain:

$$\epsilon_{CP1}(\omega) = A_1\left[-\frac{\sqrt{\omega_{g1}-\omega_{01}}}{2(\omega+i\Gamma_1)^2}\ln\left(1-\left(\frac{\omega+i\Gamma_1}{\omega_{01}}\right)^2\right) + \frac{2\sqrt{\omega_{g1}}}{(\omega+i\Gamma_1)^2}\tanh^{-1}\left(\sqrt{\frac{\omega_{g1}-\omega_{01}}{\omega_{g1}}}\right) - \frac{\sqrt{\omega+i\Gamma_1-\omega_{g1}}}{(\omega+i\Gamma_2)^2}\tan^{-1}\left(\sqrt{\frac{\omega_{g1}-\omega_{01}}{\omega+i\Gamma_1-\omega_{g1}}}\right) - \frac{\sqrt{\omega+i\Gamma_1+\omega_{g1}}}{(\omega+i\Gamma_1)^2}\tanh^{-1}\left(\sqrt{\frac{\omega_{g1}-\omega_{01}}{\omega+i\Gamma_1+\omega_{g1}}}\right)\right] \quad (6)$$

This equation contains 4 parameters: $\omega_{01}$, $\omega_{g1}$, $\Gamma_1$, and $A_1$, which have all been defined previously.

For an $M_2$ critical point, the jDOS is:

$$jDOS(\omega) \propto \left\{\begin{array}{cc} C_2 & \text{for } \omega < \omega_{g2} \\ C_2-\sqrt{\omega_{g2}-\omega} & \text{for } \omega > \omega_{g2}\end{array}\right\} \quad (7)$$

where $C_2$ is constant.

In this case, the jDOS is zero for energies below $\omega_{02}$, but is constant between $\omega_{02}$ and $\omega_{g2}$, and then decreases until it reaches zero at higher energy. Preliminary fits of our experimental data have shown that $\omega_{g2}$ is higher than 5 eV for both Au and Ag. Since this is higher than our energy window of interest, and for the sake of simplicity, we will model the jDOS as a constant from $\omega_{02}$ to infinity. The contribution to the dielectric function becomes:

$$\epsilon_{CP2}(\omega) = -\frac{A_2}{2(\omega+i\Gamma_2)^2}\ln\left(1-\left(\frac{\omega+i\Gamma_2}{\omega_{02}}\right)^2\right) \quad (8)$$

There is another set of transitions that are possible near L between the d manifold and the part of the sp band that lies above the Fermi level ($\omega_{03}$ in Figure 2b). In this case, the associated critical point would be an $M_1$ critical point at L, but with transitions restricted to energies higher than $\omega_{03}$. This results in a jDOS that is constant above $\omega_{03}$. However, since the transition at the critical point is forbidden, we expect that this contribution will be very weak. Indeed, preliminary fits have shown that the contribution from this set of transitions is negligible. For this reason, these transitions will not be taken into account in our model.

Including the Drude terms and both critical points, this model uses a total of 10 parameters to describe the frequency-dependent dielectric function of the metal. Because Au and Ag have similar band structures, we assume an identical model for both metals and their alloys, with different parameter values for each alloy composition. We also assume that every parameter evolves smoothly as a function of alloy composition, due to the smooth evolution of the dielectric function.[14]

To model the composition dependence of the fitting parameters, we use a polynomial composition function for each parameter. A linear dependence is not sufficient for most parameters, but a second-order dependence is enough to account for the behaviour of all parameters. In this case, 3 sub-parameters are needed to define the curve. The complete wavelength and

composition-dependent model therefore relies on 30 variable parameters:

$$\in(\omega, GMF) = \in_{\infty}(GMF) - \frac{(\omega_p(GMF)^2)}{\omega^2 + i\omega\Gamma_p(GMF)} + \in_{CP1}(\omega, \omega_{01}(GMF), \omega_{g1}(GMF), \Gamma_1(GMF), A_1(GMF)) + \in_{CP2}(\omega, \omega_{02}(GMF), \Gamma_2(GMF), A_2(GMF)) \quad (9)$$

Where $\varepsilon_\infty$ is the contribution from high-energy transitions, $\omega_p$ is the plasma frequency, $\Gamma_p$ is the broadening factor related to the free-electron lifetime in the Drude model, and GMF is the gold molar fraction. Each parameter in this equation is composition-dependent. There are many equivalent ways to specify the parabolic composition dependence, each requiring three points of reference. We chose to reference both pure Au and Ag compositions as well as the midpoint composition of equal parts Au and Ag. For example, we can compute the plasma frequency for any value of GMF using this equation:

$$\omega_p(GMF) = GMF^2(2\omega_{pAu} - 4\omega_{pAuAg5050} + 2\omega_{pAg}) + GMF(-\omega_{pAu} + 4\omega_{pAuAg5050} - 3\omega_{pAg}) + \omega_{pAg} \quad (10)$$

where $\omega_{pAu}$, $\omega_{pAuAg5050}$, and $\omega_{pAg}$ are the plasma frequencies for pure Au, for a 50:50 alloy, and for pure Ag, respectively. Similar composition dependence is assumed for the other fitting parameters. We note that the choice of Au, Ag, and 50:50 alloy compositions for the definition of the parabolic curve is purely for convenience. Finally, we compute the fitting parameters by comparing the model to experimental dielectric functions of five alloy compositions simultaneously.

This model represents an improvement over previous attempts, because it is based on the actual band structure of the metals in a way that forbids negative absorption. This is the first time such a model has been used to fit the dielectric function of Au–Ag alloys of arbitrary composition.

## 3. Measurement Results

**Figure 3** shows the measured real and imaginary parts of $\varepsilon$ for the five alloy thin films. At high energy, all dielectric functions are dominated by interband effects. The threshold of interband transitions shifts from about 2.5 eV for Au to about 4 eV for Ag, with a progressive shift for the alloys. This transition is also much sharper for the pure elements compared to the alloys. Intraband transitions are more important at longer wavelengths. In this region, all samples show similar behaviour for the real part of the dielectric function. The most notable difference is in the imaginary part, where alloys have a much higher absorption compared to the pure metals.

## 4. Fitting Procedure

The fitting procedure uses a genetic algorithm, which is well suited for multi-parameter optimization problems.[23] Briefly, this method involves the generation of individuals, which are vectors containing the 30 parameters to optimize. An initial

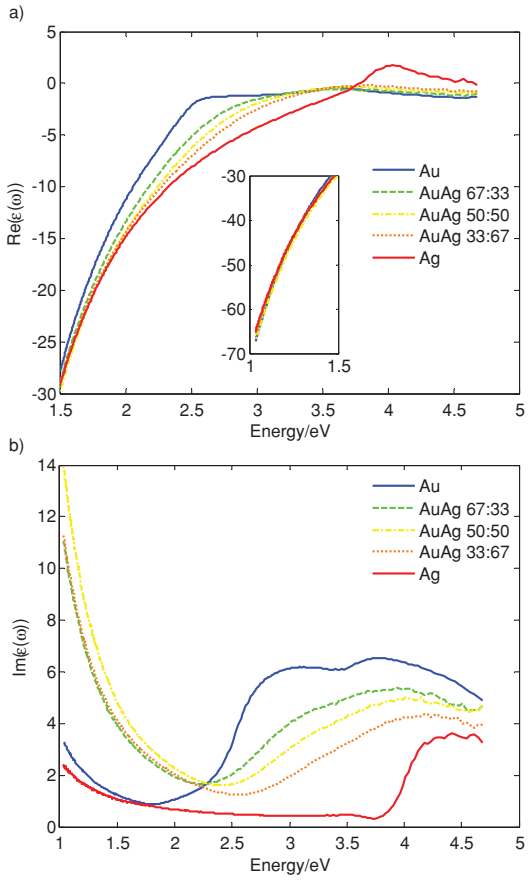


**Figure 3.** Measured a) real and b) imaginary parts of the dielectric function for 80 nm AuAg alloy thin films in the UV–NIR range. For a better visibility of the features, the real part of $\varepsilon$ has been shown on a 1.5 to 4.6 eV energy scale. The curves from 1 to 1.5 eV are shown in the inset.

population of individuals is created choosing a random value for each parameter. The fitness of each individual from the population is determined by the least-squares error, calculated between the experimentally measured dielectric function and the dielectric function modeled using the individual's parameters. The fittest individuals are the ones with the lowest least-squares error, and only these will undergo reproduction in the subsequent generation. After enough iterations, the best individual generates a solution that converges to the experimental measurements.

**Figure 4** shows the real and imaginary parts of the dielectric function for Au as predicted by the model after the fitting procedure. The agreement between the model and experiment is excellent. Note that no negative absorption is seen for the contribution of the critical points.

## 5. Discussion

### 5.1. Behaviour of the Parameters

**Table 1** lists the parameter values determined by the fit, which can be used to calculate the dielectric function in the visible range for an Au–Ag alloy of arbitrary composition.

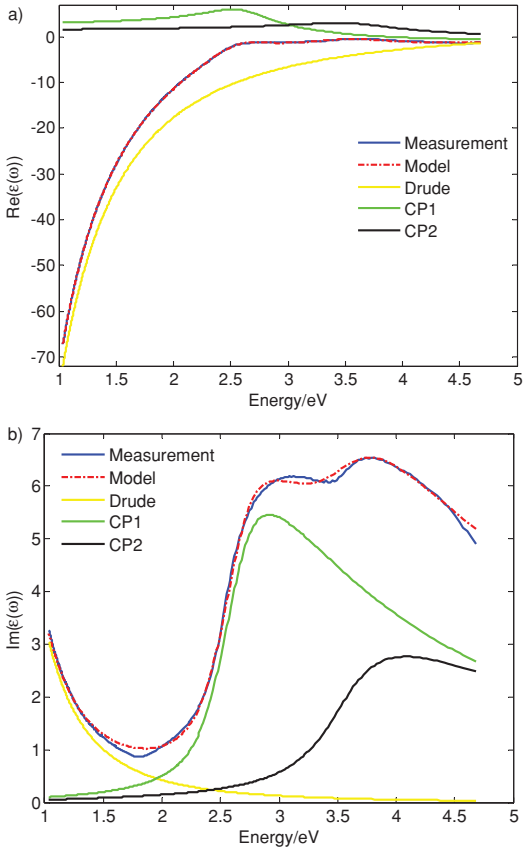


**Figure 4.** Comparison of the model with experimental data for the real a) and imaginary b) parts of $\varepsilon$ for Au. The contributions of the Drude term and both critical points are shown. For both critical points, there is no negative absorption.

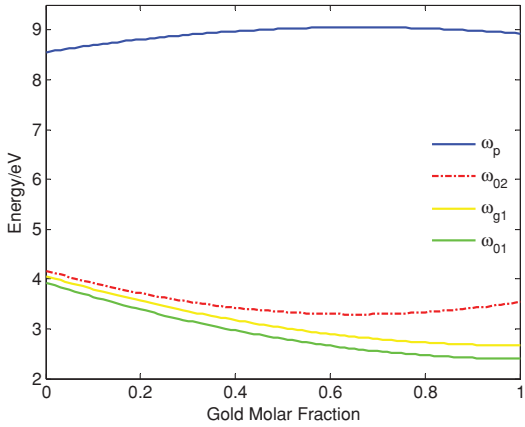


**Figure 5.** Evolution of the plasma and resonance frequencies in the model. The plasma frequency is almost constant for all alloy compositions. The threshold of transition for the first critical point is not linear, but evolves smoothly as a function of composition.

According to the Drude model, the plasma frequency $\omega_p$ is related to the density of valence electrons. Since Au and Ag share the same crystal structure and similar lattice constants, the density of valence electrons for both metals and their alloys is almost identical, resulting in comparable plasma frequencies across all compositions. As shown on **Figure 5**, the plasma frequencies predicted by our model vary by less than 5% across all compositions, and closely agree with Drude model predictions for Au and Ag using known electronic densities.[24]

Both $\omega_{01}$ and $\omega_{g1}$ have a similar behaviour, which shows that the band separation varies monotonically with alloy composition and is coherent with the linear variation of the interband transition threshold pointed out by Gaudry.[14] The relatively small variation in $\omega_{02}$ (less than 1 eV) is a consequence of the comparable band separations in Au and Ag at the L symmetry point.

In the Drude model, the imaginary part of the dielectric function is proportional to the value of $\Gamma_p$, which is itself inversely proportional to the mean free path of the conduction electrons. Since alloys are disordered materials, the random distribution of Au and Ag atoms on the crystal lattice destroys the periodicity of the structure. This lowers the mean free path of the conduction electrons for alloys, with a minimum close to the 50:50 alloy composition. This phenomenon results in a higher value of $\Gamma_p$ for alloys compared to pure metals, as shown in **Figure 6**, and explains the higher value for the imaginary part of $\varepsilon$ at long wavelengths, as pointed out earlier.

Furthermore, we observe an increase in $\Gamma_1$ and $\Gamma_2$ for alloys compared to pure metals, similar to the behaviour of $\Gamma_p$. In this case, the non-periodic structure broadens every energy state, probably resulting in a global broadening of the interband electronic transitions.

### 5.2. Comparison to Experimental Nanoparticles

In order to assess the quality of the model, we compared the extinction peaks for alloy nanoparticles predicted by the model to the measured extinction peaks for alloy particles produced experimentally. Au–Ag alloy nanoparticles of various compositions were produced by femtosecond laser ablation and alloying. This approach is described extensively elsewhere.[25] The composition of the samples runs from pure Ag to pure Au by steps of 10% in GMF. It is important to note that except for the 50:50 alloy, all of the alloys have a

**Table 1.** Fitting parameters for the dielectric function of Au–Ag alloys.

| | $\omega_p$ [eV] | $\Gamma_p$ [eV] | $\varepsilon_\infty$ | $\omega_{g1}$ [eV] | $\omega_{01}$ [eV] | $\Gamma_1$ [eV] | $A_1$ | $\omega_{02}$ [eV] | $\Gamma_2$ [eV] | $A_2$ |
|---|---|---|---|---|---|---|---|---|---|---|
| Au | 8.9234 | 0.042389 | 2.2715 | 2.6652 | 2.3957 | 0.1788 | 73.251 | 3.5362 | 0.35467 | 40.007 |
| AuAg 50:50 | 9.0218 | 0.16713 | 2.2838 | 3.0209 | 2.7976 | 0.18833 | 22.996 | 3.3400 | 0.68309 | 57.540 |
| Ag | 8.5546 | 0.022427 | 1.7381 | 4.0575 | 3.9260 | 0.017723 | 51.217 | 4.1655 | 0.18819 | 30.770 |

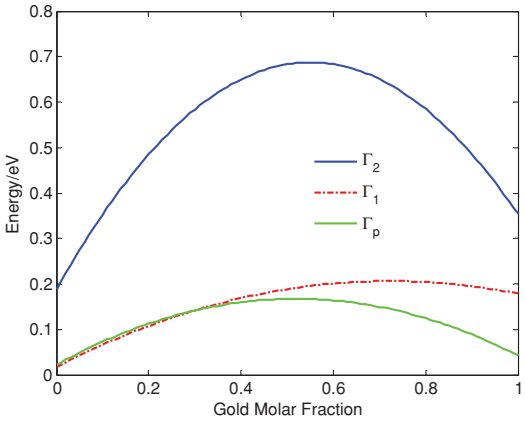


**Figure 6.** Evolution of the plasma broadening and the broadening factors of the critical points for different alloy compositions. The maximum of the plasma broadening factor is close to the 50:50 alloy.

composition different from that of the alloy thin films used to fit the model.

The particles are spherical and their mean size was determined to be around 5 nm by TEM. At these sizes, the position of the extinction peak is size-independent; however, the mean free path of conduction electrons is affected by the size of the nanoparticles, which affects the dielectric function. Because we measured and modelled the dielectric function of bulk alloys, a size-dependent correction must be applied to obtain a dielectric function representative of nanoparticles. In this case, the modification of the mean free path affects $\Gamma_p$, see Kreibig et al. for details:[26]

$$\Gamma_p(R) = \Gamma_{p\,Bulk} + \alpha\frac{h v_F}{R} \tag{11}$$

where $\Gamma_{pBulk}$ is the value obtained in our fit; $\nu_F$ is the Fermi speed of the free electrons, equal to $1.4\times10^6$ m s$^{-1}$ for Au, Ag, and their alloys;[27] $R$ is the radius of the nanoparticle; and $\alpha$ is a parameter whose value depends on the theory used for calculation, but which is close to 1. We used $\alpha = 1$ in this case, with good results.

**Figure 7** shows the comparison between the extinction spectra calculated by Mie theory using dielectric functions obtained with our model (including size correction to the dielectric function) and the measured extinction spectra for experimental nanoparticles, as a function of composition. For the calculations, the nanoparticles are assumed to be spherical (a requirement for Mie theory) with a mean size of 5 nm and a log-normal size distribution with a coefficient of variation of 20%. The insets show the positions of the maxima of the extinction peaks as well as their half width at half maxima (HWHM) (which is defined as the difference between the wavelength at the peak maximum and the wavelength at which its value has dropped to half of the maximum). We see a very good agreement in the general shape and width of the extinction peaks. The positions of the modelled peaks are within 5% of their experimental equivalent. The model does predict an almost linear shift of the plasmon peak position with composition, which is coherent with most studies of experimental alloy

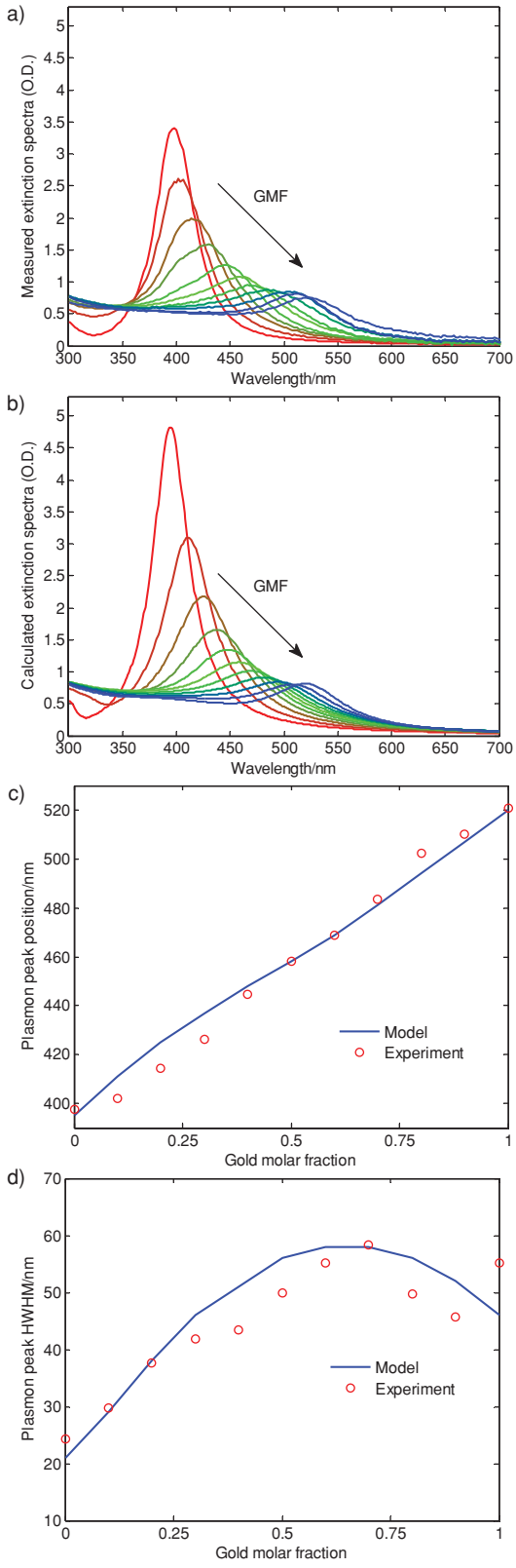


**Figure 7.** a) Measured and b) calculated extinction spectra for AuAg alloys showing excellent agreement between model and experiment, c,d) show the agreement between the plasmon peak position and the peak width respectively.

nanoparticles.[15,28,29] The most obvious difference between the experimental and calculated peaks is for pure Ag where the model predicts a higher peak. This may be due to the surface roughness and oxidation of the particles. Such effects are expected to dampen the plasmon peak.[30,31]

## 6. Conclusion

We have developed an analytic model to predict the complex dielectric function of Au–Ag alloys with arbitrary composition in the UV–vis–NIR range. The model was developed based on critical point analysis of the band structure of Au and Ag. A total of 30 parameters completely define the frequency and composition-dependent dielectric function. This model closely reproduces the dielectric function for alloy thin films measured by ellipsometry and accurately predicts optical properties of alloy nanoparticles. This capability is invaluable for quickly and accurately modelling the optical properties of alloy nanostructures.

## 7. Experimental Details

Alloy thin films were produced by co-evaporation of Au and Ag on a 1 mm thick borosilicate glass substrate. The thin film thickness is 80 nm for each sample. The sample compositions are $Au_{100}$, $Au_{67}Ag_{33}$, $Au_{50}Ag_{50}$, $Au_{33}Ag_{67}$, and $Ag_{100}$ respectively. Thin film compositions were characterized by XPS in survey mode using a VG ESCALAB 3 Mark II with a magnesium K–alpha X-ray source and a resolution of 1 eV. Dielectric functions were measured by ellipsometry using a J.A. Woollam co., VASE ellipsometer. The ellipsometric measurements were done in two steps. First, transmission through the thin film and glass substrate at normal incidence was measured from 270 to 1200 nm. Second, polarimetric reflection was measured at 3 angles (55, 65, and 75 degrees) on the same wavelength range. By modelling a thin film on a thick borosilicate glass substrate, the dielectric function of the thin film can be computed from these two measurements. The optical properties of the borosilicate glass substrate were taken from the database of the ellipsometer software. It is important to note that the film thickness was left as a fittable parameter in the computation and was determined to be $80 \pm 4$ nm for all samples.

## Supporting Information

Supporting Information is available from the Wiley Online Library or from the author. It includes a MatLAB script function that generates the dielectric function of the Au–Ag alloy, based on this model.

## Acknowledgements

The authors would like to thank Maxime Vaufleury and Suzie Poulin from the LASM at École Polytechnique for their help in the XPS measurements as well as Mathieu Maisonneuve and André-Pierre Blanchard-Dionne from the LP2L at École Polytechnique for their help with the ellipsometry measurements. The authors acknowledge the financial contribution of the Natural Sciences and Engineering Research Council of Canada.

Received: November 6, 2013
Revised: November 21, 2013
Published online: December 21, 2013

[1] X. Huang, I. H. El-Sayed, W. Qian, M. A. El-Sayed, *J. Am. Chem. Soc.* **2006**, *128*, 2115.
[2] P. K. Jain, I. H. El-Sayed, M. A. El-Sayed, *Nano Today* **2007**, *2*, 18.
[3] C. T. Nguyen, J. T. Nguyen, S. Rutledge, J. Zhang, C. Wang, G. C. Walker, *Cancer Lett.* **2010**, *292*, 91.
[4] C. Loo, A. Lin, L. Hirsch, M.-H. Lee, J. Barton, N. Halas, J. West, R. Drezek, *Technol. Cancer Res. Treat.* **2004**, *3*, 33.
[5] E. Boisselier, D. Astruc, *Chem. Soc. Rev.* **2009**, *38*, 1759.
[6] J. Baumgart, L. Humbert, É. Boulais, R. Lachaine, J.-J. Lebrun, M. Meunier, *Biomaterials* **2012**, *33*, 2345.
[7] E. C. Le Ru, P. G. Etchegoin, *Principles of Surface-Enhanced Raman Spectroscopy and Related Plasmonic Effects*, Elsevier, Amsterdam, Netherlands **2009**.
[8] J. Homola, *Anal. Bioanal. Chem.* **2003**, *377*, 528.
[9] P. B. Johnson, R. W. Christy, *Phys. Rev. B* **1972**, *6*, 4370.
[10] E. Palik, *Handbook of Optical Constants of Solids*, Academic Press, San Diego, CA, USA **1998**.
[11] H. Ehrenreich, H. Philipp, *Phys. Rev.* **1962**, *128*.
[12] K. Ripken, *Zeitschrift fur Phys.* **1972**, *250*, 228.
[13] J. Rivory, *Phys. Rev. B* **1977**, *15*, 3119.
[14] M. Gaudry, J. Lermé, E. Cottancin, M. Pellarin, J. Vialle, M. Broyer, B. Prével, M. Treilleux, P. Mélinon, *Phys. Rev. B* **2001**, *64*, 085407.
[15] S. Link, Z. L. Wang, M. a. El-Sayed, *J. Phys. Chem. B* **1999**, *103*, 3529.
[16] M. Moskovits, I. Srnová-Šloufova, B. Vlčková, *J. Chem. Phys.* **2002**, *116*, 10435.
[17] C. F. Bohren, D. R. Huffman, *Absorption and Scattering of Light by Small Particles*, Wiley-VCH Verlag GmbH, Weinheim, Germany **1998**.
[18] P. G. Etchegoin, E. C. Le Ru, M. Meyer, *J. Chem. Phys.* **2006**, *125*, 164705.
[19] P. G. Etchegoin, E. C. Le Ru, M. Meyer, *J. Chem. Phys.* **2007**, *127*, 189901.
[20] J. Leng, J. Opsal, H. Chu, M. Senko, D. E. Aspnes, *Thin Solid Films* **1998**, *313–314*, 132.
[21] M. Cardona, *Solid State Physics: Modulation Spectroscopy*, Academic Press, New York, NY, USA **1969**.
[22] website: http://exciting-code.org/, accessed: November, **2012**.
[23] M. Mitchell, *An Introduction to Genetic Algorithms*, MIT Press, Cambridge, MA, USA **1996**.
[24] N. W. Ashcroft, N. D. Mermin, *Solid State Physics*, Harcourt, Fort Worth, TX, USA **1976**.
[25] S. Besner, M. Meunier, *J. Phys. Chem. C* **2010**, *114*, 10403.
[26] U. Kreibig, M. Vollmer, *Optical Properties of Metal Clusters*, Springer-Verlag, Berlin, Germany **1995**.
[27] C. Kittel, *Introduction to Solid State Phisics*, Wiley, New York, NY, USA **1996**.
[28] I. Lee, S. W. Han, K. Kim, *Chem. Commun.* **2001**, *3*, 1782.
[29] D. Tiedemann, U. Taylor, C. Rehbock, J. Jakobi, S. Klein, W. A. Kues, S. Barcikowski, D. Rath, *Analyst* **2013**, DOI: 10.1039/c3an01463k.
[30] J. Banhart, *Phys. Rev. Lett.* **1999**, *82*, 2139.
[31] D. C. Schinca, L. B. Scaffardi, F. A. Videla, G. A. Torchia, P. Moreno, L. Roso, *J. Phys. D. Appl. Phys.* **2009**, *42*, 215102.